

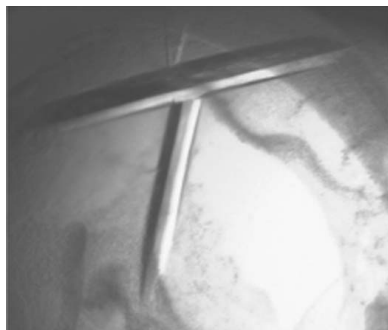
Kristin Hasselt,<sup>a‡</sup> Madhumati Sevvana,<sup>b‡</sup> Andreas Burkovski<sup>a\*</sup> and Yves A. Muller<sup>b\*</sup>

<sup>a</sup>Lehrstuhl für Mikrobiologie, Friedrich-Alexander-Universität Erlangen-Nürnberg, Staudtstrasse 5, 91058 Erlangen, Germany, and <sup>b</sup>Lehrstuhl für Biotechnik, Friedrich-Alexander-Universität Erlangen-Nürnberg, Henkestrasse 91, 91052 Erlangen, Germany

‡ These authors contributed equally to the manuscript.

Correspondence e-mail:  
aburkov@biologie.uni-erlangen.de,  
ymuller@biologie.uni-erlangen.de

Received 13 August 2009  
Accepted 10 September 2009



© 2009 International Union of Crystallography  
All rights reserved

## Crystallization and preliminary crystallographic analysis of the global nitrogen regulator AmtR from *Corynebacterium glutamicum*

AmtR, a member of the TetR family of transcription regulators, is a global regulator of nitrogen control in *Corynebacterium glutamicum*. Unlike other TetR-family members, which are regulated by small-molecule effectors, AmtR is regulated by a protein called GlnK. It has been shown that a GlnK trimer has to become adenylylated prior to formation of a complex with AmtR. The physiological function of AmtR has been very well studied, but structural characterization of the mechanistic aspects of AmtR-regulated transcription has yet to be accomplished. AmtR has successfully been crystallized in space group  $P2_12_12$ , with six molecules in the asymmetric unit and unit-cell parameters  $a = 153.34$ ,  $b = 163.10$ ,  $c = 51.93$  Å. Preliminary phases were obtained using Se-SAD.

### 1. Introduction

Almost all of the macromolecules in the bacterial cell, *e.g.* proteins, nucleic acids and cell-wall components, contain nitrogen. Thus, prokaryotes have developed elaborate mechanisms to provide an optimal nitrogen supply for metabolism and to survive situations of nitrogen limitation; these are generally subsumed under the term nitrogen control. *Corynebacterium glutamicum*, a Gram-positive soil bacterium, is used in the industrial production of amino acids (Takors *et al.*, 2007; Burkovski, 2007; Hänsler & Burkovski, 2008). Transcription of genes in response to nitrogen limitation in *C. glutamicum* is governed by the all-helical TetR-type regulator AmtR (Jakoby *et al.*, 2000; Walter *et al.*, 2007), which blocks the transcription of various genes during growth in nitrogen-rich medium.

Functionally, AmtR is one of the best characterized transcriptional regulators in *C. glutamicum*. In contrast to almost all other TetR-type proteins, which bind low-molecular-weight molecules such as tetracycline or other effectors (Ramos *et al.*, 2005), the binding of AmtR to the promoter sequences of nitrogen-controlled genes is controlled by protein-complex formation. AmtR is released from its target DNAs upon interaction with a trimeric complex of the signal transduction protein GlnK. For this protein–protein interaction, it is essential that GlnK is adenylylated at tyrosine residue 51 located within the T-loop of the protein (Nolden *et al.*, 2001; Strösser *et al.*, 2004; Beckers *et al.*, 2005). The adenylylation and deadenylylation of GlnK depends on the cellular nitrogen status and is catalysed by GlnD (Strösser *et al.*, 2004). The AmtR regulon in *C. glutamicum* comprises at least 35 genes, which encode transporters and enzymes for ammonium assimilation (*amtA*, *amtB*, *glnA*, *gltBD*, *dapD*) and the metabolism of creatinine (*codA*, *crnT*) and urea (*urtABCDE*, *ureABCEFGD*), a number of biochemically yet uncharacterized enzymes and transport systems as well as signal transduction proteins (*glnD*, *glnK*) (Beckers *et al.*, 2005; Buchinger *et al.*, 2009).

While the physiological function of AmtR has been characterized in considerable detail, its mechanistic aspects are less clear. The interaction between the DNA-binding domain of AmtR and its target DNA was studied by modelling the helix–turn–helix DNA-binding motif. The identified DNA-interacting amino acids could subsequently be verified by alanine scanning of the DNA-binding domain, purification of recombinant AmtR proteins, gel retardation and

surface plasmon resonance experiments (Muhl *et al.*, 2009). Although successful in identification of the DNA-binding epitope, a homology-derived AmtR model falls short of explaining important aspects of AmtR function: AmtR is a rare example of a TetR-family member in which the DNA-binding affinity of the repressor is modulated by a protein interaction rather than by a small metabolite. This is most likely to be caused by an allosteric coupling mechanism between the binding site for the protein GlnK and the DNA-binding sites. To our knowledge, the only other example of such a protein-regulated TetR-family member is DhaS from *Lactococcus lactis*, which is regulated by DhaQ (Christen *et al.*, 2006). Although the structure of DhaS by itself is known, little is known about the DhaQ-binding epitope on DhaS and nothing is known about the mechanism by which this protein-protein interaction modulates the DNA-binding affinity of DhaS. Regulation of AmtR appears to be even more finely tuned, since GlnK has to become adenylylated (GlnK-AMP) in order to induce AmtR with high efficiency. As a first step in the molecular and structural analysis of the AmtR-GlnK-AMP interaction and associated allosteric regulation, we successfully purified and crystallized GlnK-free and DNA-free AmtR and were able to obtain initial phases using Se-SAD.

## 2. Materials and methods

### 2.1. Protein production and purification

For the production of AmtR, 8 l LB medium was inoculated to an OD<sub>600</sub> of 0.1 using an overnight culture of *Escherichia coli* BL21 (Studier *et al.*, 1990) cells freshly transformed with plasmid pMalc2amtR. Cells were grown in LB medium with 2% glucose and 100 µg ml<sup>-1</sup> ampicillin at 310 K to an OD<sub>600</sub> of 0.5 and were induced with 0.3 mM IPTG. After 4 h incubation, the cells were harvested, resuspended in 25 ml purification buffer (20 mM Tris-HCl pH 7.4,

200 mM NaCl, 1 mM EDTA) and disrupted by sonication (Bandelin Sonoplus UW2070, Berlin). Cell debris was removed by centrifugation (14 000g, 277 K, 30 min) and the supernatant was loaded onto a 10 ml amylose-resin column (NEB, Frankfurt; GE Healthcare, Munich) and washed with ten column volumes of purification buffer; the bound fusion protein was eluted with 20 mM maltose in purification buffer. The fusion protein was then cleaved off with factor Xa (NEB, Frankfurt), producing an AmtR fragment that starts with the N-terminal sequence Thr-Ala. While the threonine residue is a remnant of the factor Xa cleavage site, the alanine residue is the first residue of the mature AmtR protein omitting the starting methionine residue. However, factor Xa cleavage is not 100% specific. In a minor fraction, a further cleavage could be observed after residue Arg14 of AmtR, as identified by MALDI-TOF MS (data not shown). Following cleavage of the fusion protein, AmtR and MBP were separated on a 16/60 Superdex 75 gel-filtration column. A total of 8.1 mg pure AmtR protein was obtained. The protein solution was adjusted to 11 mg ml<sup>-1</sup> (Sartorius Vivaspin 500, 10 000 molecular-weight cutoff) and filtered (Millipore, Ultrafree MC, 0.22 µm) before crystallization.

Since no experimental structures of close sequence homologues of AmtR (identity >20%; FFAS server; <http://ffas.ljcrf.edu/ffas-cgi/cgi/ffas.pl>) are available as search models for molecular replacement, we also purified selenomethionine-derivatized protein. For this purpose, cells (BL21/pMalamtR) were grown in M9 minimal medium with 100 µg ml<sup>-1</sup> ampicillin. From a 300 ml overnight culture, 8 l M9 medium was inoculated to an OD<sub>600</sub> of 0.1. At an OD<sub>600</sub> of 0.5–0.6, 0.5 mg ml<sup>-1</sup> amino acids were added (1 g lysine, threonine and phenylalanine and 0.5 g leucine, isoleucine, valine and selenomethionine). After 15 min incubation the cells were induced with 0.3 mM IPTG. Subsequent purification steps were carried out as described above, with the exception that all buffers additionally contained 5 mM DTT. 7.56 mg protein was obtained and was

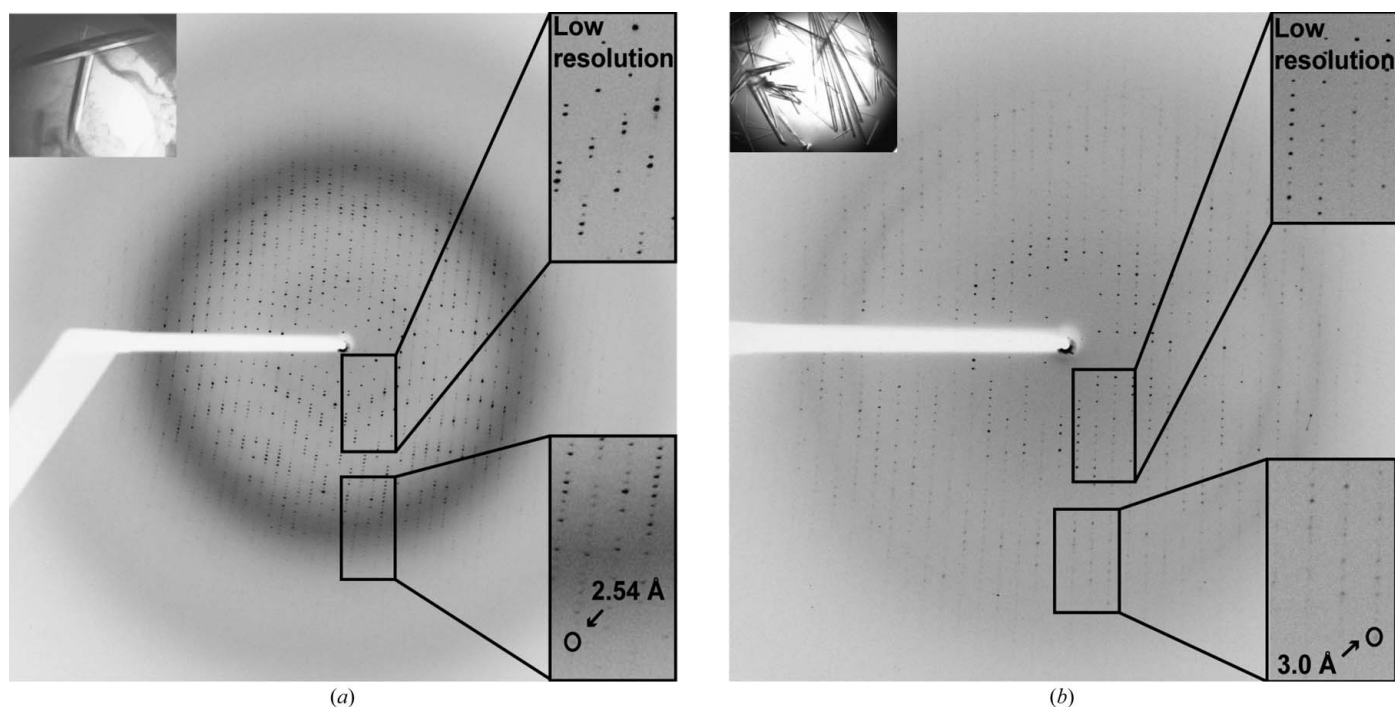


**Figure 1** (a) Needle-like crystals of wild-type AmtR grown to dimensions of 1 × 0.2 × 0.2 mm and diffraction pattern of the protein crystal, which diffracted to a maximum resolution of 2.54 Å. (b) Thin needles of selenomethionine-derivatized AmtR and associated diffraction pattern with a maximum resolution of 3.0 Å. The insets in both (a) and (b) show the high- and low-resolution limits.

concentrated to a volume of 140  $\mu\text{l}$  (Sartorius Vivaspin 500, 10 000 molecular-weight cutoff), resulting in a protein concentration of 11  $\text{mg ml}^{-1}$ . The successful incorporation of selenomethionine was confirmed *via* MALDI-TOF MS.

## 2.2. Crystallization

Native AmtR protein was subjected to extensive crystallization trials using commercially available screens (Sigma Basic Crystallization Kit and Hampton Additive Screen from Hampton Research, USA). Reproducible crystallization conditions could be identified using the hanging-drop vapour-diffusion method with the following reservoir conditions: 0.2 *M* sodium acetate, 0.1 *M* sodium citrate pH 5.6 and 20% PEG 4000. These crystals were then optimized using different additives: 4% acetonitrile, 10 *mM* betaine-HCl, 3%

methanol and 10 *mM* EDTA. In general, 700  $\mu\text{l}$  reservoir solution was used and the suspended droplets were made up of 1  $\mu\text{l}$  AmtR protein solution and 1  $\mu\text{l}$  reservoir solution. Selenomethionine-derivatized AmtR crystals were obtained using various ratios (1:2, 1:1 and 2:1) of protein and reservoir solutions.

## 2.3. Data collection and structure solution

Crystals were immersed in cryoprotectant solution (prepared by adding 250  $\mu\text{l}$  ethylene glycol to 1000  $\mu\text{l}$  reservoir solution: 0.2 *M* sodium acetate, 0.1 *M* sodium citrate pH 5.6 and 20% PEG 4000) for 30 s, mounted in a nylon loop and flash-cooled in a stream of nitrogen gas cooled to 100 K. The wild-type crystals diffracted to a maximum resolution of 2.54  $\text{\AA}$  and the selenomethionine-derivatized crystals diffracted very weakly to 3  $\text{\AA}$  at the BESSY synchrotron source

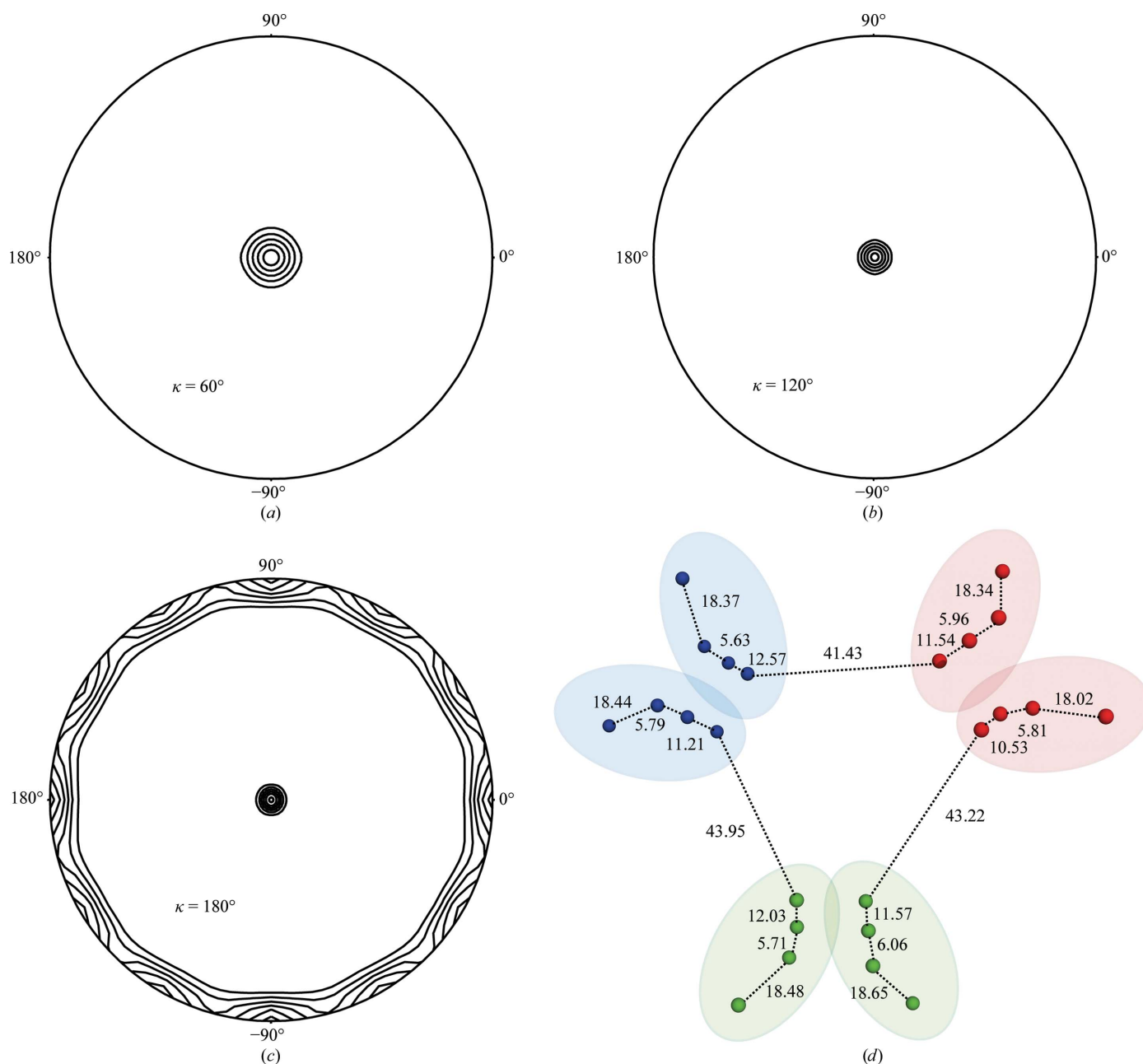


**Figure 2**  
(a–c) Self-rotation plots of the native data, showing 622 point-group symmetry. (d) Se substructure from SHELXD, showing 32 point-group symmetry.

(Berlin, Germany; Fig. 1). A single native data set and two MAD data sets were collected at 100 K (Table 1). Data were indexed and integrated using *XDS* and scaled using *XSCALE* (Kabsch, 1993). A self-rotation function was calculated using *POLARRFN* (Collaborative Computational Project, Number 4, 1994).

Since the crystals suffered from severe radiation damage, attempts to solve the selenium substructure using the individual MAD data sets failed. Therefore, we merged the peak data sets from two different crystals and performed Se-SAD. Normalized difference structure factors were calculated using *SHELXC* and the substructure was solved using *SHELXD* (Sheldrick, 2008). A first round of phase extension and density modification was carried out using *SHELXE* (Sheldrick, 2008). NCS averaging was performed using *RESOLVE* (Terwilliger, 2004) and *DM* (Cowtan, 1994).

### 3. Results and discussion

Using the two-step purification protocol described above, it was possible to produce highly pure AmtR protein with typical yields of about 1.25 mg pure protein per litre of cell culture. The purified protein could readily be used for functional characterization (Muhl *et al.*, 2009) and crystallization trials. Needle-like crystals of wild-type AmtR protein grew over a span of one month to dimensions of 1 × 0.2 × 0.2 mm (Fig. 1). Selenomethionine-derivatized crystals grew under similar conditions with different protein-reservoir ratios but were very small and fragile (Fig. 1). Their reproducibility was poorer than in the case of the wild-type protein. Diffraction data were

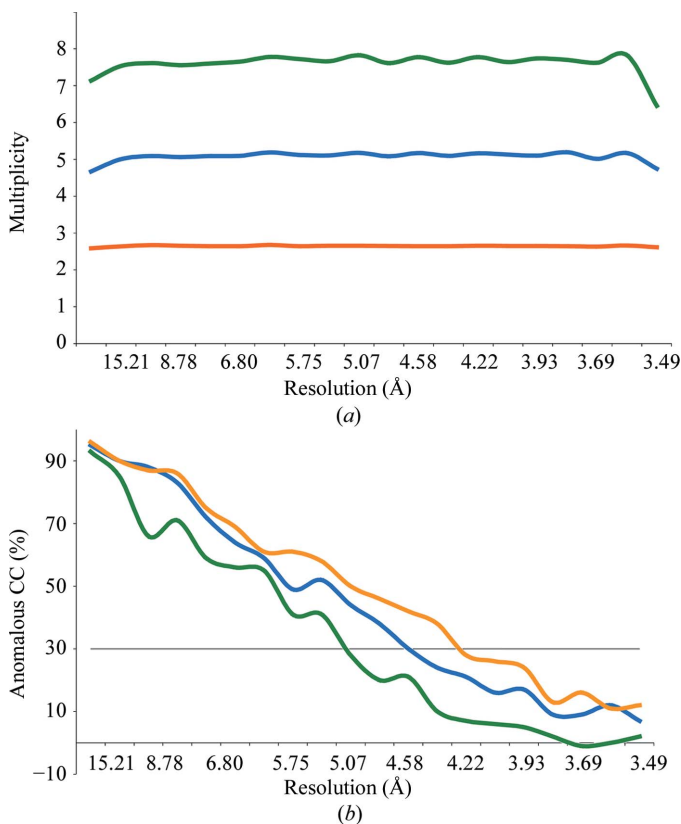


**Figure 3** Plots showing (a) multiplicity and (b) anomalous correlation coefficients for different resolution ranges. The merged data set is indicated in green, the Se-Peak1 data set in orange and the Se-Peak2 data set in blue. The resolution cutoff for solving the substructure was chosen such that the anomalous correlation coefficient was above 30%.

**Table 1** Data-collection statistics.

Values in parentheses are for the highest resolution shell.

	Native	Se-Peak1	Se-Peak2	Se-Merged
Beamline	Bessy-MX BL-14.1			
Detector	Rayonics MX-225 3 × 3 CCD detector			
Temperature (K)	100			
Wavelength (Å)	0.95373	0.97966		
Space group	<i>P</i> <sub>2</sub> <sub>1</sub> <sub>2</sub> <sub>1</sub> <sub>2</sub>			
Unit-cell parameters (Å, °)				
<i>a</i> (Å)	153.34	153.11	153.40	
<i>b</i> (Å)	163.10	163.18	163.96	
<i>c</i> (Å)	51.93	51.98	52.06	
$\alpha = \beta = \gamma$ (°)	90	90	90	
Resolution range (Å)	2.54 (2.54–2.61)	3.4 (3.4–3.49)	3.0 (3.0–3.08)	3.0 (3.0–3.08)
Unique reflections	43804 (3072)	34062 (2390)	50039 (3637)	50308 (3639)
Average multiplicity	7.05 (6.1)	5.09 (4.74)	2.62 (2.50)	6.05 (2.50)
Completeness (%)	99.6 (95.2)	98.4 (91.5)	98.9 (96.4)	99.4 (96.4)
Mean <i>I</i> / $\sigma$ ( <i>I</i> )	24.39 (3.17)	13.60 (4.25)	10.51 (2.01)	9.86 (1.13)
<i>R</i> <sub>merge</sub> <sup>†</sup> (%)	7.2 (63.2)	10.7 (38.2)	9.4 (52.7)	15.1 (52.7)
<i>R</i> <sub>meas</sub> <sup>‡</sup> (%)	7.8 (69.1)	11.9 (42.9)	11.9 (67.4)	16.4 (67.2)
<i>R</i> <sub>merged,r</sub> <sup>§</sup> (%)	9.5 (55.5)	12.3 (40.5)	21.0 (90.8)	17.3 (91.7)
Wilson <i>B</i> value (Å <sup>2</sup> )	50.381	49.19	48.712	61.26

<sup>†</sup>  $R_{\text{merge}} = \frac{\sum_{hkl} \sum_i |I_i(hkl) - \langle I(hkl) \rangle|}{\sum_{hkl} \sum_i I_i(hkl)}$ , where  $I_i(hkl)$  is the intensity measurement for reflection  $hkl$  and  $\langle I(hkl) \rangle$  is the mean intensity of symmetry-related reflections and replicates. <sup>‡</sup>  $R_{\text{meas}}$  is defined as  $\frac{\sum_h [n_h / (n_h - 1)]^{1/2} \times \sum_i^n |I_i(h) - I_{h,i}|}{\sum_h \sum_i^n I_{h,i}}$  (Diederichs & Karplus, 1997). <sup>§</sup>  $R_{\text{merged},r}$  is defined as  $\frac{\sum |A_{I,h,r} - A_{I,h,q}| / 0.5 \sum (A_{I,h,r} + A_{I,h,q})}{\sum (A_{I,h,r} + A_{I,h,q})}$  (Diederichs & Karplus, 1997).

collected from cryocooled (100 K) crystals using a MAR CCD detector on beamline BL-14.1 at the Bessy synchrotron source. Data were collected using 1° oscillations with the crystal-to-detector distance set to 210 mm for the native data set and 310 mm for the selenomethionine-derivatized crystals. Analysis of merging statistics and systematic absences indicated that the crystals belonged to space group *P*<sub>2</sub><sub>1</sub><sub>2</sub><sub>1</sub><sub>2</sub>, with unit-cell parameters *a* = 153.34, *b* = 163.10, *c* = 51.93 Å. The calculated molecular mass of the protein is 24.4 kDa per subunit. Assuming six monomers per asymmetric unit in space group *P*<sub>2</sub><sub>1</sub><sub>2</sub><sub>1</sub><sub>2</sub> yields a Matthews coefficient of 2.17 Å<sup>3</sup> Da<sup>-1</sup> with a solvent content of 43.2%. Analysis of the self-rotation function of the native data calculated in the resolution range 20–3.5 Å using an integration radius of 35 Å indicated the presence of 622 point-group symmetry (Figs. 2a, 2b and 2c).

Since the selenomethionine-derivatized crystals were quite thin and fragile, the inflection-point data sets exhibited severe radiation damage. Therefore, we tried to solve the structure using Se-SAD. Initial attempts to solve the substructure by Se-SAD using individual peak data sets and concomitant phase extension using *SHELXE* did not give successful solutions. In order to increase the multiplicity and completeness of the data set and thereby the quality of the anomalous signal, we merged the two peak data sets for further calculations (Table 1). Unexpectedly, *I*/ $\sigma$ (*I*) did not increase in the merged data set, hinting that the merged data set was not necessarily of better quality than the individual data sets. It is possible that it was solely the fact that the analysis of the anomalous correlation coefficients of the merged data set (Fig. 3) suggested a lower resolution cutoff (Sheldrick, 2008) that enabled us to identify the Se substructure with the merged data set rather than with the individual data sets during prior attempts.

Each AmtR molecule contains four methionines; therefore, a search for 24 selenium positions using *SHELXD* (Sheldrick, 2008) yielded 24 heavy-atom positions with correlation coefficients (all/best) of 51.97/29.61. The substructure shows 32 point-group symmetry. The 622 point-group symmetry observed in the self-rotation function is generated by a crystallographic twofold axis parallel to the noncrystallographic threefold axis (Fig. 2). This agrees well with the

expected six molecules (or three dimers) per asymmetric unit, as can be seen in Fig. 2(d). We also obtained an initial electron-density map using *SHELXE* with a pseudo-free CC of 55.71% and a contrast and connectivity of 0.527 and 0.830, respectively (Sheldrick, 2008), which showed scattered electron density for some of the helices (data not shown). NCS operators were calculated using the heavy-atom positions and the map was NCS-averaged in *RESOLVE*. The resulting electron-density map allows the tracing of some of the helices but needs still to be improved either by the collection of higher resolution SeMet data and/or NCS averaging and phase extension. The crystals are also being optimized in order to collect higher resolution native data.

We would like to thank Uwe Mueller from BESSY (Berlin, Germany) for help with data collection. MALDI-TOF MS analyses of purified AmtR were kindly carried out by Stephan Müller (Lehrstuhl für Bioverfahrenstechnik, Technical Faculty, University Erlangen-Nuremberg). This work was supported by the Deutsche Forschungsgemeinschaft (SFB473).

## References

- Beckers, G., Strösser, J., Hildebrandt, U., Kalinowski, J., Farwick, M., Krämer, R. & Burkovski, A. (2005). *Mol. Microbiol.* **58**, 580–595.
- Buchinger, S., Strösser, J., Rehm, N., Hänssler, E., Hans, S., Bathe, B., Schomburg, D., Krämer, R. & Burkovski, A. (2009). *J. Biotechnol.* **140**, 68–74.
- Burkovski, A. (2007). *J. Microbiol. Biotechnol.* **17**, 187–194.
- Christen, S., Srinivas, A., Bahler, P., Zeller, A., Pridmore, D., Bieniossek, C., Baumann, U. & Erni, B. (2006). *J. Biol. Chem.* **281**, 23129–23137.
- Collaborative Computational Project, Number 4 (1994). *Acta Cryst.* **D50**, 760–763.
- Cowtan, K. (1994). *Int CCP4/ESF-EACBM Newsl. Protein Crystallogr.* **31**, 34–38.
- Diederichs, K. & Karplus, P. A. (1997). *Nature Struct. Biol.* **4**, 269–275.
- Hänssler, E. & Burkovski, A. (2008). *Corynebacteria: Genomics and Molecular Biology*, edited by A. Burkovski, pp. 183–201. Norwich: Caister Academic Press.
- Jakoby, M., Nolden, L., Meier-Wagner, J., Krämer, R. & Burkovski, A. (2000). *Mol. Microbiol.* **37**, 964–977.
- Kabsch, W. (1993). *J. Appl. Cryst.* **26**, 795–800.
- Muhl, D., Jessberger, N., Hasselt, K., Jardin, C., Sticht, H. & Burkovski, A. (2009). *BMC Mol. Biol.* **10**, 73.
- Nolden, L., Ngouoto-Nkili, C. E., Bendt, A. K., Krämer, R. & Burkovski, A. (2001). *Mol. Microbiol.* **42**, 1281–1295.
- Ramos, J. L., Martínez-Bueno, M., Molina-Henares, A. J., Teran, W., Watanabe, K., Zhang, X., Gallegos, M. T., Brennan, R. & Tobes, R. (2005). *Microbiol. Mol. Biol. Rev.* **69**, 326–356.
- Sheldrick, G. M. (2008). *Acta Cryst.* **A64**, 112–122.
- Strösser, J., Lüdke, A., Schaffer, S., Krämer, R. & Burkovski, A. (2004). *Mol. Microbiol.* **54**, 132–147.
- Studier, F. W., Rosenberg, A. H., Dunn, J. J. & Dubendorff, J. W. (1990). *Methods Enzymol.* **185**, 60–89.
- Takors, R., Bathe, B., Rieping, M., Hans, S., Kelle, R. & Huthmacher, K. (2007). *J. Biotechnol.* **129**, 181–190.
- Terwilliger, T. (2004). *J. Synchrotron Rad.* **11**, 49–52.
- Walter, B., Hänssler, E., Kalinowski, J. & Burkovski, A. (2007). *J. Mol. Microbiol. Biotechnol.* **12**, 131–138.